

DUST DESTRUCTION RATES AND LIFETIMES IN THE MAGELLANIC CLOUDS

TEA TEMIM^{1,2}, ELI DWEK¹, KIRILL TCHERNYSHYOV³, MARTHA L. BOYER^{1,4}, MARGARET MEIXNER^{3,5},
CHRISTA GALL^{6,7}, JULIA ROMAN-DUVAL⁵

Accepted to The Astrophysical Journal, Nov 17, 2014

ABSTRACT

The nature, composition, abundance, and size distribution of dust in galaxies is determined by the rate at which it is created in the different stellar sources and destroyed by interstellar shocks. Because of their extensive wavelength coverage, proximity, and nearly face-on geometry, the Magellanic Clouds (MCs) provide a unique opportunity to study these processes in great detail. In this paper we use the complete sample of supernova remnants (SNRs) in the MCs to calculate the lifetime and destruction efficiencies of silicate and carbon dust in these galaxies. We find dust lifetimes of 22 ± 13 Myr (30 ± 17 Myr) for silicate (carbon) grains in the LMC, and 54 ± 32 Myr (72 ± 43 Myr) for silicate (carbon) grains in the SMC. The significantly shorter lifetimes in the MCs, as compared to the Milky Way, are explained as the combined effect of their lower total dust mass, and the fact that the dust-destroying isolated SNe in the MCs seem to be preferentially occurring in regions with higher than average dust-to-gas (D2G) mass ratios. We also calculate the supernova rate and the current star formation rate in the MCs, and use them to derive maximum dust injection rates by asymptotic giant branch (AGB) stars and core collapse supernovae (CCSNe). We find that the injection rates are an order of magnitude lower than the dust destruction rates by the SNRs. This supports the conclusion that, unless the dust destruction rates have been considerably overestimated, most of the dust must be reconstituted from surviving grains in dense molecular clouds. More generally, we also discuss the dependence of the dust destruction rate on the local D2G mass ratio and the ambient gas density and metallicity, as well as the application of our results to other galaxies and dust evolution models.

Subject headings: dust, extinction - infrared: ISM - ISM: individual objects (MAGELLANIC CLOUDS) - ISM: supernova remnants

1. INTRODUCTION

The evolution of dust grains in galaxies is driven by their formation rate in the different stellar sources, their processing by supernova (SN) blast waves, and by their reconstitution in dense interstellar clouds. Dust formation sites include the ejecta of core collapse and Type Ia supernovae (CCSNe, SNIa, respectively), novae, and mass outflows from evolved stars in the Asymptotic Giant Branch (AGB) phase of their evolution and Wolf-Rayet (WR) stars. An important issue is the nature of interstellar dust. Is it entirely made of refractory elements that thermally condensed in stellar ejecta, or does it also contain heavy elements that accreted onto these refractory cores in the dense phases of the interstellar medium (ISM)?

These questions were first raised with the realization that the interstellar elemental depletion pattern

correlated with the condensation temperature (Field 1974), suggesting that thermal condensation in the stellar sources drives the evolution of dust. An equally good correlation of the elemental depletion pattern with the first ionization potential was suggested by Snow (1975) as evidence that dust was primarily grown by accretion in the ISM. This issue was first quantitatively addressed by Dwek & Scalo (1980) who examined the balance between the formation rates of dust in CCSNe and AGB stars and their destruction rate by SN remnants (SNRs) in the framework of a chemical evolution model. They noted that any deficiency between the rate of dust formation and destruction may necessitate grain growth by accretion in the ISM, in order to explain the abundance of dust in the diffuse ISM, as inferred from the elemental depletion pattern. This conclusion was confirmed by detailed calculations of the grain destruction rates (Jones et al. 1996; Slavin 2014), and more detailed chemical evolution models (Dwek 1998; Tielens 1998; Zhukovska et al. 2008; Calura et al. 2010) for the solar neighborhood.

The need for the ISM accretion to explain the inferred dust abundance in local and high-redshift galaxies was also confirmed in chemical evolution models (Valiante et al. 2009; Gall et al. 2011a; Dwek & Cherchneff 2011a; Dwek et al. 2011). The problem is primarily the consequence of the fact that CCSNe are net destroyers of dust, that is, they destroy more dust in the remnant phase of their evolution than they form in the ejecta. When this difference is not made up by dust production in AGB stars, the “missing” dust must be grown onto the surviving refractory grain cores in the ISM. Only in very high

¹ Observational Cosmology Lab, Code 665, NASA Goddard Space Flight Center, Greenbelt, MD 20771, USA

² CRESST, University of Maryland-College Park, College Park, MD 20742, USA

³ Department of Physics and Astronomy, The Johns Hopkins University, 366 Bloomberg Center, 3400 North Charles Street, Baltimore, MD 21218, USA

⁴ Oak Ridge Associated Universities (ORAU), Oak Ridge, TN 37831, USA; tea.temim@nasa.gov

⁵ Space Telescope Science Institute, 3700 San Martin Drive, Baltimore, MD 21218, USA

⁶ Department of Physics and Astronomy, Aarhus University, Ny Munkegade 120, DK-8000 Aarhus C, Denmark

⁷ Dark Cosmology Centre, Niels Bohr Institute, University of Copenhagen, Juliane Maries Vej 30, DK-2100 Copenhagen, Denmark

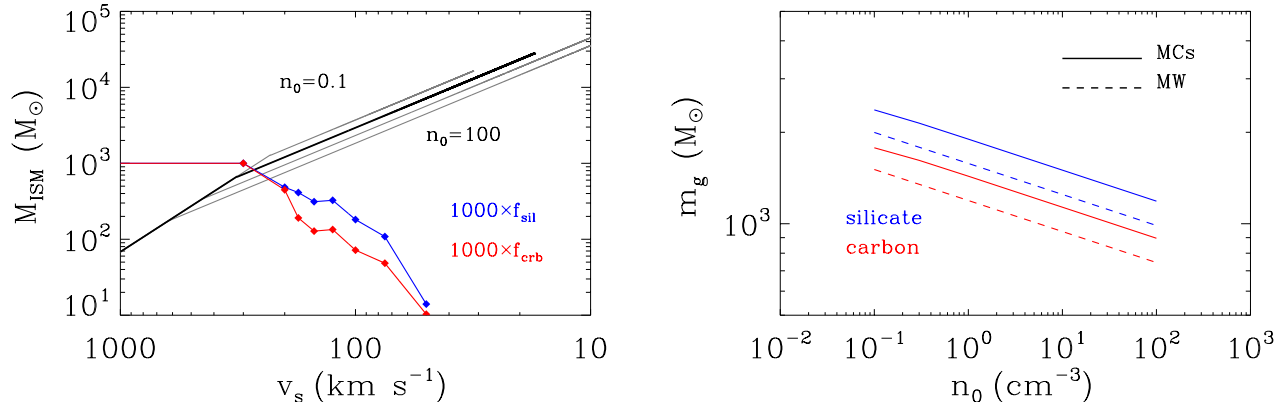


FIG. 1.— **Left panel:** Mass of ISM material swept up by a pressure driven SNR, as a function of shock velocity. The grey curves represent swept-up masses for different ISM densities ranging from $n_0 = 0.1 - 100 \text{ cm}^{-3}$, while the black curve represents $n_0 = 1 \text{ cm}^{-3}$. The blue (red) curves represent grain destruction efficiencies for silicate (carbon) grains, multiplied by a factor of 1000 for display purposes. The efficiencies were taken from Table 4 of Jones et al. (1996), with additional calculations for intermediate velocities provided by Slavin (private communication). **Right panel:** The total effective swept-up mass m_g as a function of ISM density for silicate (blue) and carbon (red) grains. The total mass m_g at each density is the convolution of the swept-up ISM mass M_{ISM} and the grain destruction efficiency $f_d(v_s)$, integrated over the shock velocity. It can be seen that m_g is only weakly dependent on the ISM density ($\propto n^{-0.107}$). The solid line represents m_g values for the MCs, while the dashed line represents values for the MW, which is lower due to its higher metallicity.

redshift galaxies, in which the dust to gas mass ratio is $\lesssim 10^{-4}$, are CCSNe net producers of interstellar dust, alleviating the need to reconstitute the dust in the ISM (Dwek et al. 2014).

The question of the imbalance between the dust destruction and production rates can be uniquely addressed by studies of the Large and Small Magellanic Clouds, LMC and SMC, respectively. These galaxies are the best astrophysical laboratories to study the lifecycle of dust in galaxies. Their proximity (50 kpc, e.g. Schaefer (2008) and 62 kpc, Szcwzyk et al. (2009)) permits detailed studies of individual stars and stellar populations. These can be used to derive their star formation history (Harris & Zaritsky 2004, 2009), and dust production rates from carbon- and oxygen-rich stars (Srinivasan et al. 2009; Matsuura et al. 2009; Boyer et al. 2010; Riebel et al. 2012; Boyer et al. 2012; Matsuura et al. 2013). Their almost face-on geometry reveals a fairly complete sample of SNRs (Badenes et al. 2010). Most importantly, recent far infrared (IR) observations of the MCs with the *Herschel* Space Observatory (Meixner et al. 2013), allow us to observationally determine the properties of the environment into which each SNR is expanding, and therefore determine the most reliable current rate of grain destruction in the MCs.

In this paper we use the observationally determined ISM density and dust-to-gas (D2G) mass ratio around a nearly complete sample of SNRs in the MCs to calculate the global rate of grain destruction and the corresponding dust lifetimes. For comparison, we also calculate a maximum rate of grain formation in the quiescent outflows of AGB stars and the explosively ejected material in CCSN events. The main purpose is to determine if the balance between the injection and destruction of dust in the MCs is consistent with currently observed dust emission.

The paper is organized as follows. In §2 we present the general equations for calculating the grain destruction rate by SNRs and identify the parameters that determine this rate. In §3 we describe how we derive each of

the required parameters, and use the HI gas and *Herschel* Space Observatory IR images to calculate the ISM density and dust-to-gas (D2G) mass ratio of the medium into which each of the SNRs expand, and the masses of dust destroyed during the evolution of the SNRs. In §4, we give the corresponding dust destruction rates and lifetimes and discuss how they compare to those of the Milky Way. In §5, we discuss how our results can be applied to other galaxies and dust evolution models. In §6, we derive upper limits on the dust formation rates in AGB and CCSNe, and compare them to the dust destruction rates that we derive in this work. Our major goal is to determine if there is a discrepancy in the balance between the dust formation and destruction rates in the MCs that may require an additional source of dust. The astrophysical implication of our results are discussed in §7.

2. GENERAL EQUATIONS

Isolated SNRs expanding into the ISM destroy interstellar grains by thermal-kinetic sputtering and vaporizing grain-grain collisions. There are several distinct lines of evidence for grain destruction and processing in shocks: (1) X-ray observations showing changes in the elemental abundances and ionization structure of heavy elements in the postshock flow (Vancura et al. 1994; Raymond et al. 2013); (2) UV observations showing changes in the depth of the 2200 Å extinction feature and in the slope of the extinction across the shock (Seab & Shull 1983); (3) analysis of IR observations that show changes in the grain size distribution before and after the shock (Arendt et al. 2010; Sankrit et al. 2010), (4) significantly lower than average D2G mass ratio in LMC SNRs (Williams et al. 2006; Borkowski et al. 2006; Williams et al. 2011); and (5) differences in dust density maps along the line of sight to the LMC SNRs (Lakićević et al. 2014).

The dust mass destroyed by a single SNR, m_d , can be expressed by (Jones et al. 1994; Dwek et al. 2007):

$$m_d = Z_d m_g = Z_d \int_{v_i}^{v_f} f_d(v_s) \left| \frac{dM_{\text{ISM}}}{dv_s} \right| dv_s. \quad (1)$$

where Z_d is the D2G mass ratio of the local ISM into which the remnant expands, m_g is the effective mass of ISM gas that is completely cleared of dust by a single SNR, dM_{ISM}/dv_s is the rate at which the ISM is swept up by the SNR as a

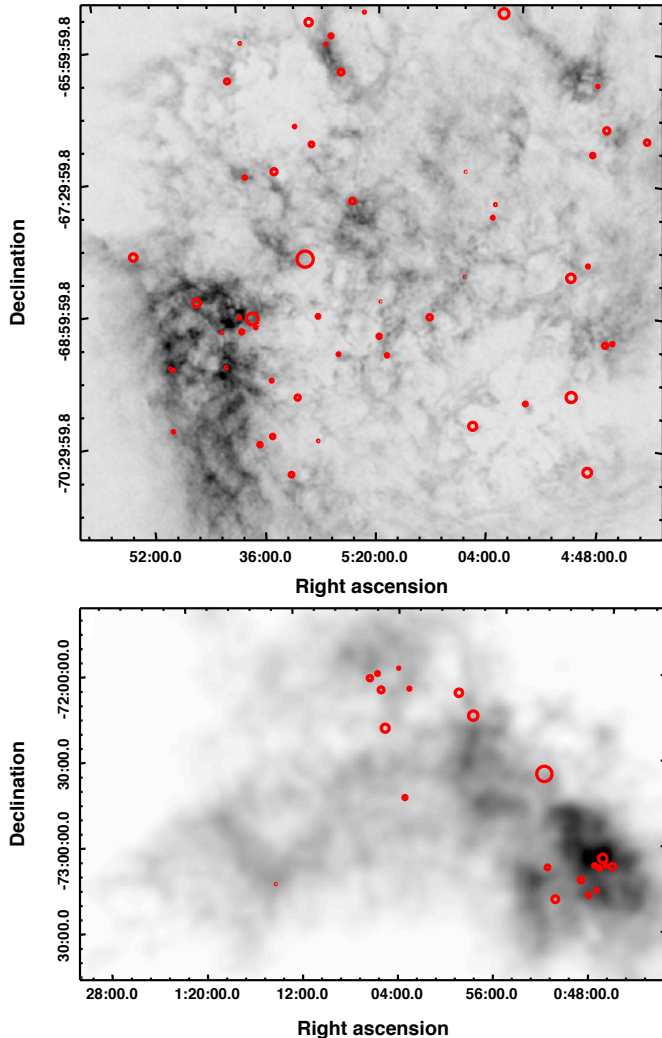


FIG. 2.— HI surface density maps of the LMC (Kim et al. 1999) and SMC (Stanimirovic et al. 1999) with the positions of observed SNRs overlaid as red circles. The size of the circles represents the measured SNR sizes as listed in Badenes et al. (2010) and Lakićević et al. (2014).

function of shock velocity v_s , and $f_d(v_s)$ is the fraction of dust that is destroyed as a function of shock velocity. For example, models of the pre- and postshock *Spitzer* Infrared Spectrograph (IRS) spectra of Puppis A (Arendt et al. 2010) and the Cygnus Loop (Sankrit et al. 2010) show that ~ 25 – 30% of the grains are destroyed in $\sim 500 \text{ km s}^{-1}$ shocks. The limits of the integral extend from the initial velocity of the remnant, v_i to v_f , its final velocity when the ejecta reaches the random velocities of the ISM.

For our analysis, we compute the SNR evolution and dM_{ISM}/dv_s values using the pressure-driven snowplow model of Cioffi et al. (1988). The results are shown in Figure 1 (left panel), where the gray and black curves represent the total mass of ISM material swept up by an SNR as a function of shock velocity for ISM densities ranging from $n_0 = 0.1 - 100 \text{ cm}^{-3}$, and an explosion energy $E_0 = 10^{51} \text{ erg}$.

The right panel of Figure 1 shows the total effective swept-up mass m_g as a function of ISM density for silicate and carbon grains, using the grain destruction efficiencies from (Jones et al. 1996, Table 4), with additional calculations for intermediate velocities provided by Slavin (2014, private communication, in prep). The total mass m_g is simply the convolution of the swept-up ISM mass M_{ISM} and the grain destruc-

tion efficiency $f_d(v_s)$ in the left panel of Figure 1, integrated over the shock velocity. The weak dependence of m_g on the ISM density implies that the primary factor that determines the dust mass destroyed by an SNR, m_d , is the D2G mass ratio in the preshocked ISM.

The dust lifetime τ_d at the current epoch can be written as:

$$\tau_d = \frac{M_d}{\bar{m}_d R_{SN}} \quad (2)$$

where M_d is the total dust mass in the galaxy, R_{SN} is the total (CCSN + Type Ia) supernova rate, and $\bar{m}_d = \sum m_d / N_{SNR}$, the mass of refractory elements initially locked up in dust, averaged over the total number of SNRs in the galaxy N_{SNR} . In rest of the paper, a bar above a symbol will indicate an appropriate average value over the total number of SNRs in the galaxy.

The current grain destruction rate, dM_d/dt , is given by:

$$\frac{dM_d}{dt} = \frac{M_d}{\tau_d} = \bar{m}_d R_{SN}. \quad (3)$$

For a given explosion energy, E_0 , the rate of grain destruction depends on: (1) $f_d(v_s)$, the grain destruction efficiency; (2) n_0 and Z_d , the density and D2G mass ratio, respectively, of the preshocked ISM into which the SNR is expanding; and (3) R_{SN} , the supernova rate. To determine the dust lifetime, we also need to know the total mass of dust in the galaxies $M_d(t)$. In this work, we use observationally determined values for M_d , and n_0 and Z_d for all confirmed SNRs, to calculate the value of the average destroyed dust mass \bar{m}_d , the dust lifetime τ_d , and the global dust destruction rate $dM_d(t)/dt$ for the Magellanic Clouds. Below, we outline the derivation method and results for each of the parameters.

3. ANALYSIS & RESULTS

3.1. SNR Sample

For our analysis, we used a list of all known SNRs in the LMC and SMC (e.g. Chu & Kennicutt 1988; Williams et al. 1999; Filipović et al. 2005; Blair et al. 2006; Badenes et al. 2010; Seok et al. 2013; Maggi et al. 2014; Lakićević et al. 2014). Badenes et al. (2010) carefully assessed the completeness of the SNR sample, and concluded that the list is a fairly complete sample that should not be missing a large number of objects. Following their study, four new X-ray selected SNRs were confirmed in the LMC by Maggi et al. (2014). Tables 1 and 2 list the names, coordinates, and diameters of all confirmed SNRs in the MCs. The list contains 61 SNRs in the LMC and 23 SNRs in the SMC. SNR diameters were measured from X-ray observations, when available, and from the best available alternative, when not. The spatial distribution of SNRs, along with their spatial sizes are shown in Figure 2. The positions and sizes are indicated by the red circles, and overlaid onto the HI surface density maps of the LMC (Kim et al. 1999) and SMC (Stanimirovic et al. 1999).

3.2. The ISM Density

The ISM density determines the rate at which the ISM mass is swept up at any given shock velocity, and hence overall the grain destruction efficiency by SNRs. To derive the pre-shock density of the ISM surrounding each SNR in the LMC and SMC, we assumed that they are expanding into a neutral hydrogen medium. We therefore extracted HI column density values in annuli at each SNR position. The HI maps were convolved to the *Herschel* SPIRE $500 \mu\text{m}$ image ($14''/\text{pixel}$) for consistency, and values were extracted from square annuli centered at each SNR, with the inner square side equal to $1 \times \text{SNR diameter}$, and the outer square side equal to $4 \times \text{SNR diameter}$. For SNRs that were smaller than one resolution

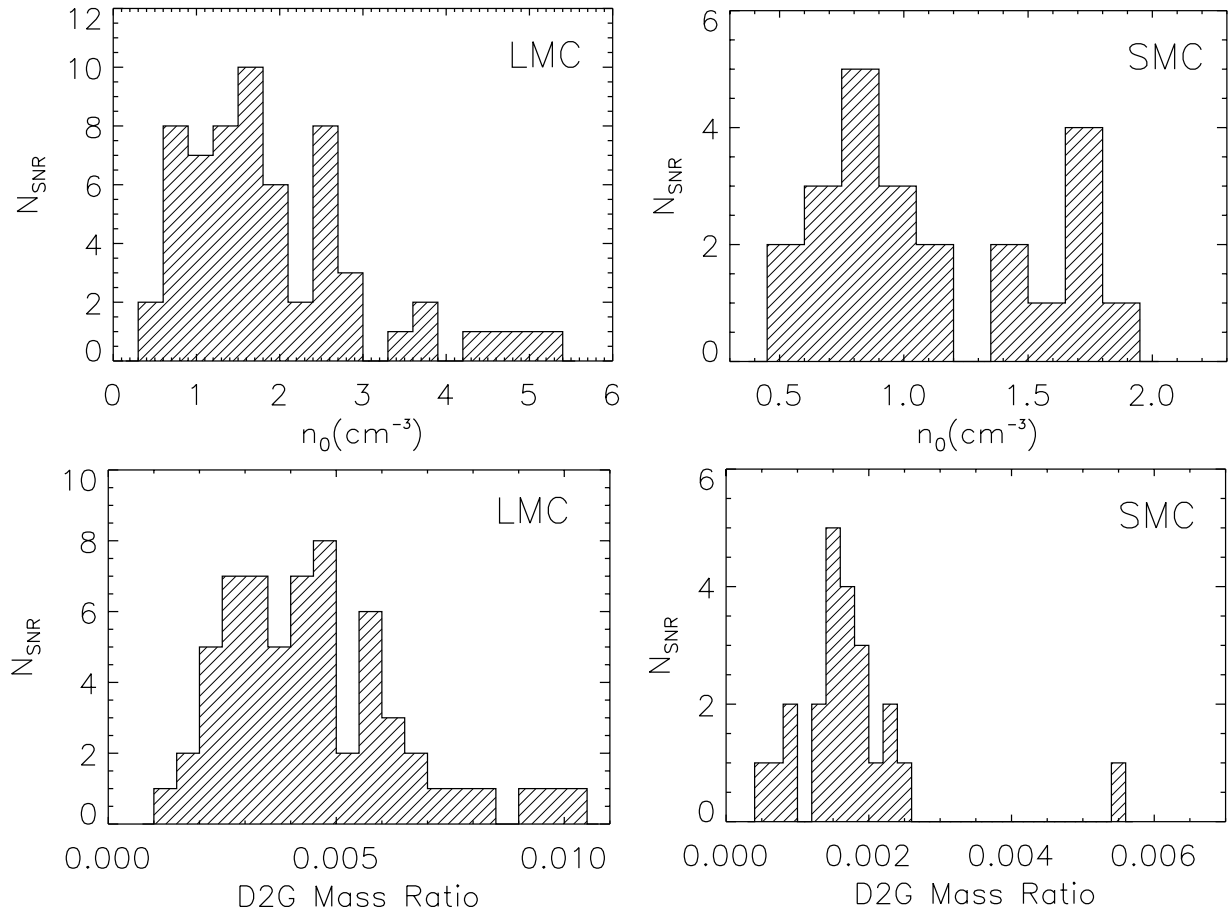


FIG. 3.— The histograms show the distribution of ambient gas densities (assuming a disk thickness of 0.4 kpc for the LMC and 2.0 kpc for the SMC) and D2G mass ratios for regions surrounding each of the SNRs.

element, values were extracted from a 9×9 pixel region, minus the central pixel. The average HI column density N_H from each of these regions for both LMC and SMC remnants is listed in Tables 1 and 2.

In order to obtain an absolute gas density into which the SNRs are expanding, we need to divide N_H by the thickness of the gas disks of the LMC and SMC. We adopt an LMC gas disk thickness of 0.4 kpc (Kim et al. 1999), and an SMC gas disk thickness of 2.0 kpc (Stanimirović et al. 2004), both based on measurements from HI observations of the MCs. In order to explore the dependence of our results on the choice of disk thickness, we computed dust destruction rates and lifetimes for a range of disk thickness values, 0.05–1.6 kpc for the LMC, and 1.0–4.0 kpc for the SMC. The upper limits for the disk thickness values were chosen based on the LMC and SMC depth estimates from observations of Cepheids and RR Lyrae stars (Haschke et al. 2012a,b).

Figure 3 (top) shows the distribution of absolute densities for both the LMC and SMC. These densities are also listed in Tables 1 and 2. The mean density n_0 around the SNR sample in the LMC and SMC as function of disk thickness is listed in Table 3.

3.3. Total Gas and Dust Masses in the Magellanic Clouds

A map of the dust mass distribution and the total mass of dust in the LMC were recently derived by Gordon et al. (2014), using a parametrized representation of the dust properties. Since we are interested in determining the separate contributions from silicate and carbon dust, which were not computed in previous works, we recalculated the dust masses

using the dust optical constants from (Li & Draine 2002) for silicate, and (Zubko et al. 1996) for amorphous carbon dust. The 70–500 μm infrared fluxes were taken with the *Herschel* PACS and SPIRE instruments, and are presented in Meixner et al. (2013).

To fit the dust models to the data, we adopted two physical constraints on the dust. The first uses the LMC and SMC elemental abundances (Tchernyshyov et al. 2014, and references therein) to constrain the relative silicate-to-carbon dust mass ratio to 2.9 for the LMC, and 4.0 for the SMC. The second constraint uses the optical properties of the two dust species to constrain the temperature ratio between carbon and silicate dust. When exposed to the general interstellar radiation field in the local solar neighborhood, carbon dust attains a temperature that is about 1.2 times higher than the silicate dust.

Figure 4 shows the fits to the SEDs of the LMC and SMC. The best fit temperatures and masses are listed in Table 4. We derived a temperature of 22.4 K (26.9 K) for silicate (carbon) dust in the LMC, and 19.0 K (22.8 K) for silicate (carbon) dust in the SMC. The resulting total dust masses are $7.0 \times 10^5 M_\odot$ and $2.0 \times 10^5 M_\odot$ for the LMC and SMC, respectively. The individual masses for the silicate (carbon) dust components are $5.2 \times 10^5 M_\odot$ ($1.8 \times 10^5 M_\odot$) for the LMC, and $1.6 \times 10^5 M_\odot$ ($4.0 \times 10^4 M_\odot$) for the SMC. Our total mass estimates are consistent with the masses derived from a parametric fit to the SED of the LMC by Gordon et al. (2014) that yielded a total dust mass of $\sim 7.3 \times 10^5 M_\odot$, somewhat lower than the values of $\sim 3.6 \times 10^6$, $\sim 1.2 \times 10^6 M_\odot$, and $\sim 1.7 \times 10^5 M_\odot$, derived by Bot et al. (2010), Leroy et al.

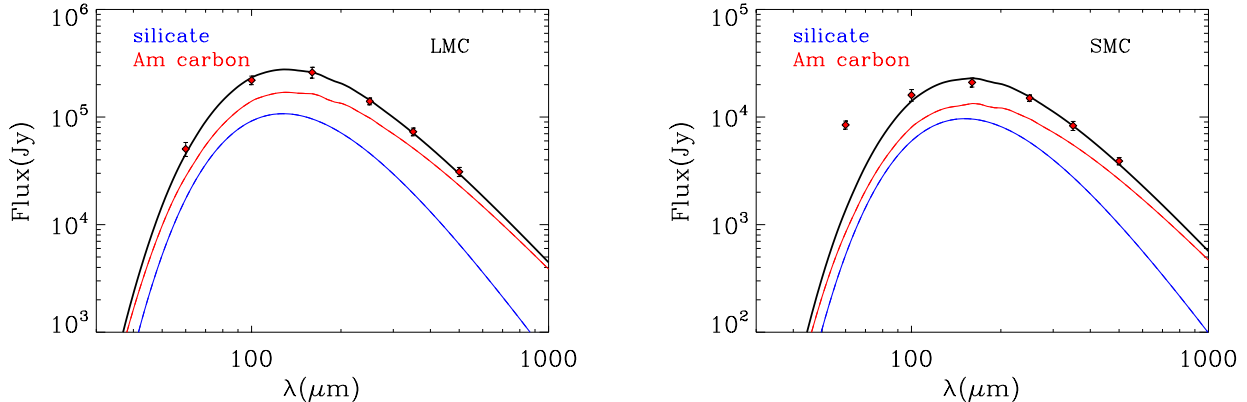


FIG. 4.— Constrained two component fits to the SEDs of the LMC and SMC. See Section 3.3 for details and Table 4 for best fit masses and temperatures.

(2007), and Bernard et al. (2008), respectively.

3.4. Dust-to-Gas Mass Ratios Around the SNRs

To calculate the D2G mass ratio in the ISM around each SNR, we extracted the 70–500 μm infrared fluxes from the *Herschel* PACS and SPIRE maps (Meixner et al. 2013), for the same annular regions surrounding each SNR as described in Section 3.2. We then fitted each of the 84 SEDs with a two-component dust model with the same carbon-to-silicate dust mass and temperature ratios used for the global SED fits (see Section 3.3). We divided the best-fit dust mass for each grain species individually by the total HI gas mass in each annular region. The resulting total D2G mass ratios are shown in Figure 3 and listed in Tables 1 and 2. Of the total dust mass, 74% (26%) is in the form of silicate (carbon) in the LMC, and 80% (20%) in the form of silicate (carbon) in the SMC. The D2G mass ratio does not depend on the choice of disk thickness, since the volume for the gas and dust masses simply cancels out.

The determination of the dust mass in the HI gas assumes single temperatures for silicate and carbon dust, ignoring the possible presence of a colder dust component that may reside in molecular clouds. Allowing for the presence of a cold dust component may reduce the dust mass attributed to the HI gas. To check the effect of our approximation, we modeled the SED of two select regions characterized by the largest CO column density with two dust components. The temperature of the first, warm component was allowed to vary between 18 and 40 K, and that of the cold dust component between 6 and 18 K. The results showed that even when the cold component dominates the dust mass, it makes a negligible contribution to the total SED, and has therefore little effect on the dust mass attributed to the HI gas, which is the only relevant mass for calculating the grain destruction rate by SNRs. However, the presence of dust in molecular clouds can alter the total dust mass reservoir, M_d , and thus the dust lifetime, but since the molecular gas constitutes only 10% of the gas mass in the MCs, the effect of cold dust on the dust lifetime is not significant.

Given the H I mass of $4.0 \times 10^8 M_\odot$ for the LMC and $2.5 \times 10^8 M_\odot$ for the SMC (Roman-Duval et al. 2014), and our total HI-associated dust masses derived for the LMC and SMC, we find a global D2G ratios of 1.8×10^{-3} and 8.0×10^{-4} for the LMC and SMC, respectively. The average D2G ratios around the observed SNRs are a factor of 2–3 higher, 4.5×10^{-3} and 1.7×10^{-3} for the LMC and SMC, respectively. Table 4 lists both the average global G2D value, and the average local value around the SNRs.

3.5. Effective Swept-up Mass

Given the model for the evolution of the SNR, the grain destruction efficiency, and the ambient ISM density, we first calculated the value of m_g for individual SNRs. Figure 5 shows the histograms of effective swept up gas mass m_g for the entire SNR sample for both carbon and silicate grains, and an assumed gas disk thickness of 0.4 kpc for the LMC and 2.0 kpc for the SMC. The corresponding values for the individual SNRs are listed in Tables 1 and 2. The first important thing to note is that the distribution of m_g is fairly narrow for any given disk thickness, implying that spatial variations in the HI column density in the MCs have a minor effect on m_g . The mean values and standard deviations of the distributions for different disc thickness values are listed in Table 3. For any given disk thickness value, the standard deviation of m_g is on the order of only 7% of the mean. This essentially means that the dust mass destroyed by each SNR (m_d) varies only with the local D2G mass ratio, and that m_d can roughly be estimated by taking the average value of m_g in Table 3, and multiplying it by the local value of Z_d . The dependence of the effective gas mass m_g on density (i.e. disk thickness) is approximately a power-law of the form $m_g \propto n_0^{-0.107}$.

Since the SNR evolution depends on the metallicity of the surrounding ISM that affects the cooling of the gas, the effective swept-up gas mass m_g also has a metallicity dependence. Based on Cioffi et al. (1988), we find that $m_g \propto \zeta_m^{-0.15}$, where ζ_m is the metallicity normalized to its solar value, and taken to be equal to 0.3 for the MCs. For comparison, m_g as a function of density for the Milky Way ($\zeta_m = 1.0$) is shown in the right panel of Figure 5. If the average metallicity around the observed SNRs in the MCs is higher than the average global metallicity, similar to the higher than average G2D, then the corresponding m_g values will be lower by 10–13 %.

3.6. Dust Mass Destroyed by Individual SNRs

The total mass of dust destroyed by each SNR, m_d is simply derived by multiplying m_g by the total D2G mass ratio in the local SNR environment. The total mass of silicate and carbon dust destroyed by each SNR is then given by their relative contribution to the total dust mass. The histogram of the resulting destroyed dust masses for each SNR for both carbon and silicate grains are shown in Figure 5 and listed in Tables 1 and 2.

The shapes of the distributions of the destroyed dust masses in Figure 5 are mainly determined by the spatial variations in the D2G mass ratio in the LMC and SMC. Since m_g does not show a strong dependence on the gas density into which the SNR expands, the variations in m_d are mainly caused by

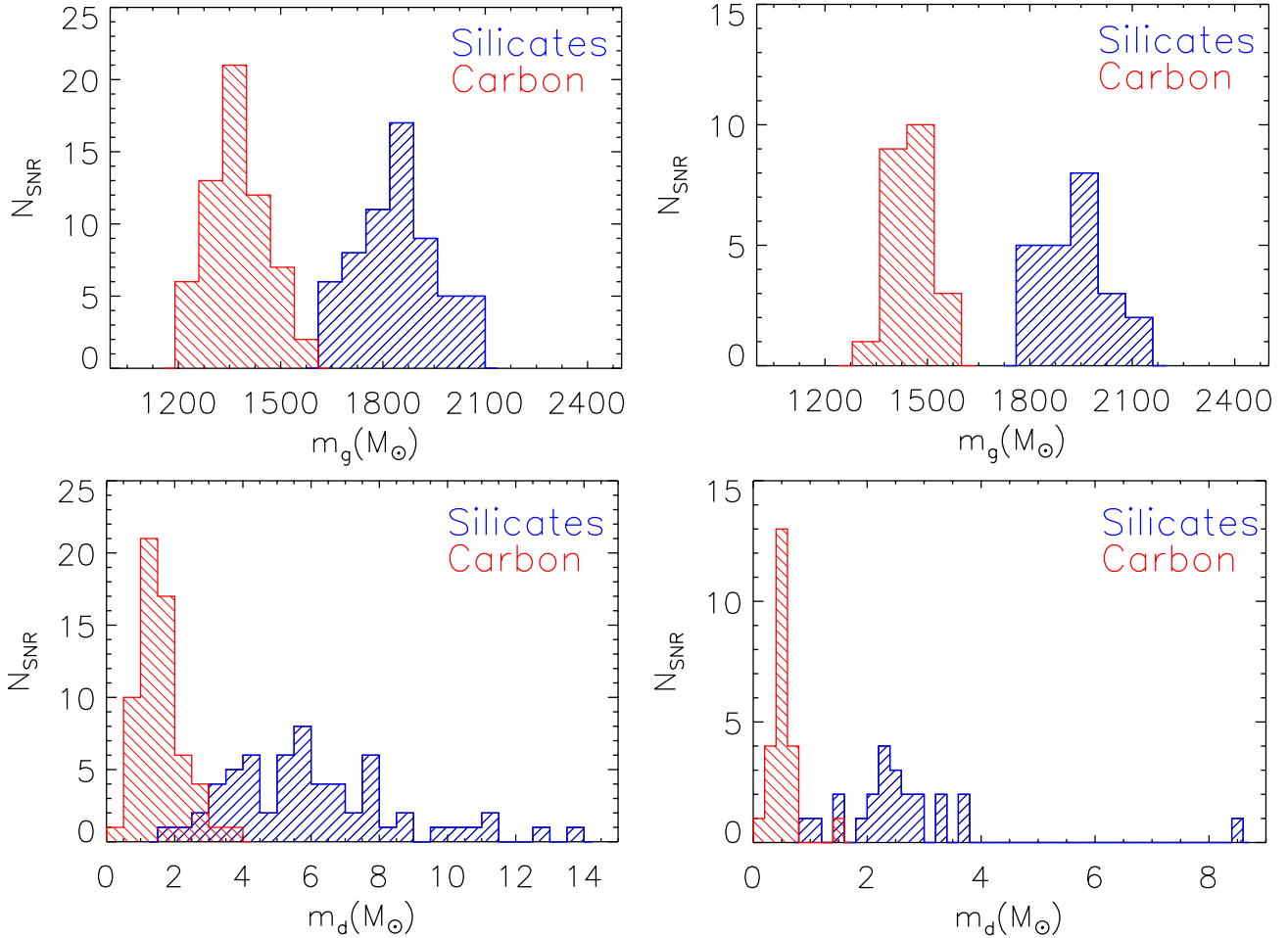


FIG. 5.— **Top:** Histograms showing the effective gas mass \bar{m}_g for the LMC (left) and SMC (right) SNRs using the silicate and carbon grain compositions. **Bottom:** Histograms showing the total amount of dust mass destroyed \bar{m}_d by each SNR in the LMC (left) and SMC (right) for silicate and carbon grain compositions. A disk thickness of 0.4 kpc was assumed for the LMC, and 2.0 kpc for the SMC, and a metallicity factor $\zeta_m = 0.3$.

the variations in the D2G mass ratio.

The average destroyed dust mass values for all SNRs as a function of disk thickness (or density) are listed in Table 3 and shown in Figure 6. The weak dependence of \bar{m}_d on gas density can be translated to a dependence on disk thickness d as $\bar{m}_d \propto d^{0.107}$. Since it is linearly dependent on m_g , it will have the same metallicity dependence, given by $\bar{m}_d \propto \zeta_m^{-0.15}$.

3.7. The Supernova Rate

The supernova rate can be derived from the observed number of SNRs, N_{SNR} , from the relation:

$$R_{\text{SN}} = \frac{N_{\text{SNR}}}{\tau_{\text{vis}}}, \quad (4)$$

where τ_{vis} is the visibility time of the SNR. This rate is accounts for only the “isolated” SNRs that we observe, and not any clustered SNRs that might have expanded inside giant or supergiant bubbles and escaped detection. As we will discuss in the next section, these clustered SNRs do not affect the dust destruction and production rates that we calculate, and are therefore not included in the SN rate. Maoz & Badenes (2010) presented a physical model in which they adopted the epoch spent by a remnant in the Sedov (adiabatic) phase of its evolution as the remnant visibility time. We also adopt this definition of the visibility time for our analysis, but use the pressure-driven SNR model by Cioffi et al. (1988).

Figure 7 shows the evolution of the SNR radius as a function of time for different ISM densities. The red segment of the curve represents the Sedov phase of the evolution of the remnant, and the dashed line the radiative phase. The visibility time depends on the ISM density, and is given by: $\tau_{\text{vis}} = 2 \times 10^4 n_0^{-4/7}$ yr. For our adopted disk thickness values of 0.4 kpc for the LMC and 2.0 kpc for the SMC correspond to an average density around the SNRs of 2 cm^{-3} and 1 cm^{-3} for the LMC and SMC, respectively. This leads to an average visibility time of 16.3×10^3 yr and 20.7×10^3 yr for the LMC and SMC, respectively. Our values are consistent with those of Badenes et al. (2010), who derived a visibility time of $\approx (14 - 20) \times 10^3$ yr, based on various density tracers for the MCs,

Based on the above equation, R_{SN} will have a $n_0^{-4/7}$ on density, and $d^{4/7}$ dependence on disk thickness. The values of R_{SN} as a function of disk thickness for the LMC and SMC are listed in Table 3. Given the number of confirmed SNRs, the average ISM densities for the nominal disk thickness values, and the visibility times, we derive SN rates of $\sim 3.75 \times 10^{-3}$ and $\sim 1.11 \times 10^{-3} \text{ yr}^{-1}$, for the LMC and SMC, respectively. These rates are lower than the Harris & Zaritsky (2009) SN rates, due to the fact that we only consider the observed isolated SNRs, and ignored cluttered SNR that give rise to giant and supergiant bubbles in the MCs. The values of R_{SN} as a function of disk thickness are listed in Table 3, and the nomi-

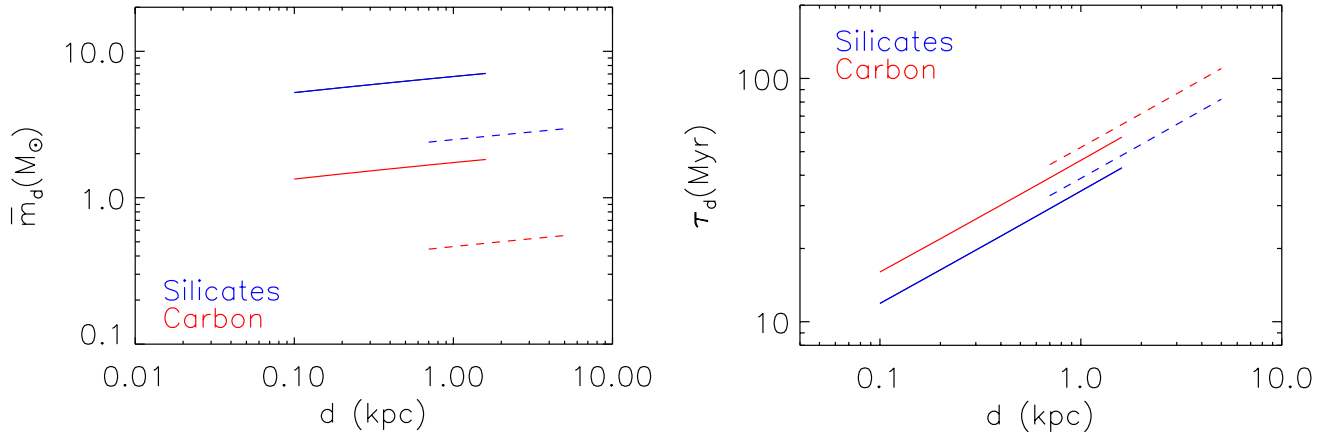


FIG. 6.— Average mass of dust destroyed per SN (left) and the average dust lifetime (right), as a function of the disk thickness, assuming a metallicity factor $\zeta_m = 0.3$. The red and blue lines represent silicate and carbon grains, respectively, while the solid (dashed) lines represent LMC (SMC) values.

nal value and the functional dependence of n_0 (or d) are listed in Table 4.

3.8. The Effect of SNR Clustering

The presence of superbubbles in the MCs (Kim et al. 1999; Stanimirovic et al. 1999) suggests that a fraction of all CCSNe created at any given time occur in a cluster environment. There are 103 giant and 23 supergiant shells catalogued in the LMC (Kim et al. 1999), and 495 giant and nine supergiant shells in the SMC (Staveley-Smith et al. 1997; Stanimirovic et al. 1999). The presence of these bubbles suggests that there exists a population of CCSNe that has escaped detection. Consequently, any SFR derived from the rate of isolated SNRs will be lower than the absolute SFR, and for this reason, our derived SN rate for the observed SNRs is lower than the values found in Harris & Zaritsky (2009).

Our rationale for using the lower SN rate, calculated from observed SNRs, is that clustered SNe have a negligible effect on the dust destruction and injection rates. Only the first massive star that explodes in the cluster will destroy the ambient dust. The remaining CCSNe will be expanding in a medium that has been cleared of dust by the first. Clustered CCSN have therefore a very low grain destruction rate compared to an identical number of isolated SNRs. The effect of correlated CCSNe therefore does not affect our dust destruction rate that was observationally derived from isolated SNRs. Similarly, clustered CCSNe do not significantly contribute to the dust injection rate, since any subsequent SN will destroy the dust produced by the previous one.

An important issue is if the observed isolated SNRs will overlap before their shock velocity drops below 50 km s^{-1} , the threshold for grain destruction. If there is significant overlap in the volumes of the ISM that the SNRs sweep up, then we may have overestimated the dust destruction rate. In order to check this, we computed the SNR radii for a time at which all the dust destruction by the SNR has occurred. These radii are basically the radii at which each SNR has swept up an m_g amount of gas. The resulting radii sizes range from 0.25 – 8 times the current SNR radius, suggesting that some SNRs in the sample have already stopped destroying dust, while others will continue to destroy dust until they reach a radius several times larger than the current one. The extreme case is SN 1987A, which will continue to destroy the ambient dust up to a radius of ~ 80 times the current SNR radius. We overlaid these evolved SNRs sizes onto the H I maps of the LMC and SMC, and found that there is no overlap in the encompassing volumes, and that the dust destruction rate has not been overestimated due to this effect.

4. DUST LIFETIME AND DESTRUCTION RATES IN THE MAGELLANIC CLOUDS

The dust lifetime, τ_d (Equation 2), calculated using the total dust mass for each grain species, the supernova rate R_{SN} , and the average destroyed dust mass per SN (\bar{m}_d), are all summarized in Table 4. For the chosen gas disk thickness values and a metallicity of $\zeta_m = 0.3$, the dust lifetimes for the LMC and SMC are $22 \pm 13 \text{ Myr}$ ($30 \pm 17 \text{ Myr}$) and $54 \pm 32 \text{ Myr}$ ($54 \pm 32 \text{ Myr}$) for silicate (carbon dust), respectively. This corresponding dust destruction rates are $2.3 \times 10^{-2} M_\odot \text{ yr}^{-1}$, ($5.9 \times 10^{-3} M_\odot \text{ yr}^{-1}$) for silicate (carbon) dust in the LMC, and $3.0 \times 10^{-3} M_\odot \text{ yr}^{-1}$ ($5.6 \times 10^{-4} M_\odot \text{ yr}^{-1}$) for silicate (carbon) dust in the SMC. The dependence of the dust lifetime and destruction rate on disk thickness and metallicity factor is $d^{0.464} \zeta_m^{-0.207}$ and $d^{-0.464} \zeta_m^{0.207}$, respectively (see Tables 3 and Table 4). The plot of τ_d as a function of d for the entire range of disk thickness values is shown in Figure 6. The dependence of the dust lifetimes and destruction rates on metallicity is also listed in Table 4.

4.1. Comparison to the Milky Way

In a uniform ISM, with a constant D2G mass ratio, the dust lifetime is independent of the total dust mass, and can be written as: $\tau_d = M_g / (\bar{m}_g R_{SN})$. Since \bar{m}_g is only a weak function of the ambient density in which an SNR is expanding, and the LMC values of M_g and R_{SN} are similar to that in the solar neighborhood, one would expect similar dust lifetimes in these two systems. However, our results show that the lifetimes of the silicate and carbon dust in the LMC and SMC are about an order of magnitude less than the ~ 400 and $\sim 200 \text{ Myr}$ derived by Jones & Nuth (2011) for the respective dust species in the solar neighborhood. As shown below, the reasons for this difference is the lower dust mass in the MCs, that the D2G mass ratio is not uniform, and that SNRs expand preferentially into an ISM with a higher than average D2G mass ratio.

The gas surface density and total (Type Ia and CCSN) rates in the solar neighborhood are $\sim 10 M_\odot \text{ pc}^{-2}$ and $\sim 0.016 \text{ pc}^{-2} \text{ Gyr}^{-1}$, respectively (Rana 1991; Dickey et al. 1993; Cappellaro 1996; Tammann et al. 1994), giving an M_g/R_{SN} ratio of $6.2 \times 10^{11} M_\odot \text{ yr}$. For an ISM density of 1 cm^{-3} , the value used by Jones & Nuth (2011) to calculate the dust lifetimes, and a metallicity $\zeta_m = 1.0$, we get values of $\bar{m}_g = 1600 M_\odot$ and $1200 M_\odot$, for silicates and amorphous carbon, respectively. Using eq. (2) we derive dust lifetimes of 375 Myr and 500 Myr for these respective dust species. Our global approach is therefore capable of reproducing the lifetimes derived by the more detailed models to within a factor

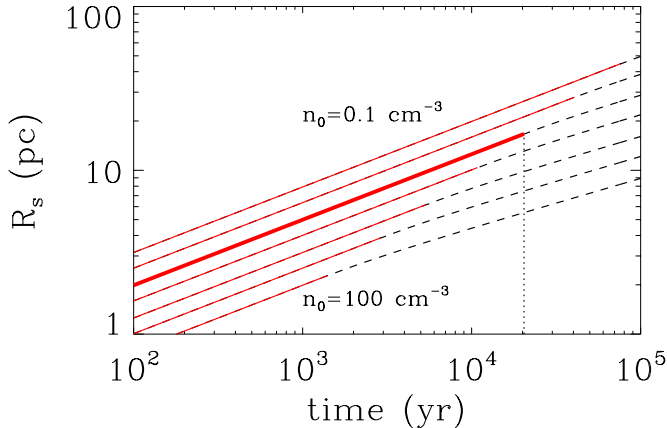


FIG. 7.— Radius of a pressure driven SN as a function of time and ISM densities, for a metallicity of $\zeta_m = 0.3$. The red and the black-dashed parts of the curve represent the Sedov and radiative phases of the remnant’s evolution, respectively. The time spent in the Sedov phase is the visibility time of the remnant. The curves represent ISM densities of 0.1, 0.3, 1.0, 3.0, 10, 30, and 100 cm^{-3} . The bold line corresponds to a remnant expanding into a medium with $n_0 = 1 \text{ cm}^{-3}$, which has a visibility time of $2 \times 10^4 \text{ yr}$.

of two.

For the LMC and SMC, the M_g/R_{SN} ratio is equal to $1.1 \times 10^{11} M_\odot \text{ yr}$ and $2.3 \times 10^{11} M_\odot \text{ yr}$, respectively, where we adopted an H I mass of $4.0 \times 10^8 M_\odot$ for the LMC and $2.5 \times 10^8 M_\odot$ for the SMC (Roman-Duval et al. 2014). Even in a uniform ISM with a constant D2G mass ratio, we would expect LMC and SMC dust lifetimes to be about ~ 6 and ~ 3 times lower than those of the solar neighborhood.

An additional difference between the dust lifetimes in the MCs and solar neighborhood stems from the assumption that the D2G mass ratio is constant throughout the ISM. The average D2G mass ratio, M_d/M_g is equal to 1.8×10^{-3} and 8.0×10^{-4} for the LMC and SMC, respectively. Table 4 shows that the D2G mass ratios of the ISM into which the SNRs are expanding are larger by an average factor of 2 – 3 compared to the global D2G mass ratio, even though the standard deviation on these values indicates a significant spread (see Table 4). Since core-collapse SN progenitors explode in the vicinity of other massive stars, it perhaps may not be surprising for their SNRs to be found in ISM environments that are more enriched in metals and dust. Since the average SN rate in the MCs is comparable to that in the solar neighborhood, we conclude that the lower dust lifetimes in the MCs are the results of their lower total dust mass and the fact that a significant fraction of SNRs seems to expand into an ISM with a higher than average D2G mass ratio.

5. APPLICATION TO OTHER GALAXIES AND DUST EVOLUTION MODELS

The SN rate that we are using to calculate dust destruction lifetimes, listed in Tables 3 and 4, is the SN rate derived from the isolated SNRs that we are currently observing, including both CC and Type Ia explosions. This SN rate is lower than the absolute SN rate that one may derive from the SFR of Harris & Zaritsky (2009), due to the fact that we leave out any correlated SNe that may have occurred inside large bubbles, and are not expected to destroy a significant amount of dust.

In order to apply our results for another epoch in the MCs or another galaxy for which the isolated SNR population is not resolved, one needs to first calculate the nominal CCSN rate from the SFR given by: $R_{SN}(t) = \psi(t)/m_*$, where $\psi(t)$ is the SFR, and m_* is the mass of stars generated per CCSN event (Dwek & Cherchneff 2011b). To calculate the effective rate of dust destroying SNR we need to take the clustering of CCSN into account, since only field SNRs will destroy the

dust, and the presence of Type Ia SNR. The rate of SN that destroy the dust at any epoch t , is then given by:

$$R_{SN}(t) = \left[\frac{\psi(t)}{m_*} \right] (1 - f_{cl} + f_{Ia}) \quad (5)$$

where f_{cl} is the fraction of CCSN that are clustered, and f_{Ia} is the fraction of Type Ia to CCSN.

Given a SN rate, Equations (2) and (3) can be used to calculate the dust lifetime and destruction rate, where the mass destroyed by an average SN can be estimated by $\bar{m}_d = \bar{Z}_d \bar{m}_g$. Here, \bar{Z}_d is the average D2G mass ratio of the ISM into which the SNe expand, which can be higher than the global D2G mass ratio of the galaxy.

Chemical evolution models usually take \bar{m}_g to be constant because of its weak dependence of ambient density. However \bar{m}_g also depends on the metallicity of the ambient medium into which the SNRs expand, since it determines the post-shock cooling of the gas, and therefore the evolution of the remnant. These two effects should be considered in future dust evolution models. The value of \bar{m}_g should be adjusted for the desired metallicity and average density of the galaxy, according to Table 4.

6. DUST PRODUCTION RATES BY CCSNE AND AGB STARS

6.1. Dust Production Rate by Type Ia SN

Theoretically, calculations by Nozawa et al. (2011) show that dust can form in these objects. However, the results show that because of the high expansion velocity and low mass of the ejecta, the resulting grain sizes are very small ($\lesssim 100 \text{ \AA}$). Furthermore, the ejecta is less likely to be clumpy, so that all dust that may have formed is expected to be destroyed by the reverse shock Nozawa et al. (2011).

Observationally, searches for dust in remnants of Type Ia SNe, including Kepler (Blair et al. 2007; Williams et al. 2012), RCW 86 (Williams et al. 2011), SN 1006 (Winkler et al. 2013), and Tycho (Williams et al. 2013), have yielded negative results. That no significant grain formation takes place in Type Ia SNe was later confirmed by *Herschel* observations of Kepler and Tycho (Gomez et al. 2012). We therefore ignore Type Ia SN as sources of dust.

6.2. Dust Production Rate by CCSNe

In contrast to Type Ia SNe, there is considerable evidence for the formation of dust in the ejecta of CCSNe. CCSNe have relatively short main sequence lifetimes, $< 40 \text{ Myr}$ for a $8 M_\odot$ progenitor, compared to the lifetime of an average AGB star. We will therefore assume that the CCSN event occurs promptly after the birth of its progenitor. The dust production rate can then be written as:

$$\left[\frac{dM_d}{dt} \right]_{CCSN} = \bar{Y}_d R_{CCSN} \quad (6)$$

where \bar{Y}_d is the CCSN yield averaged over the stellar initial mass function (IMF), and $R_{CCSN} = N_{CCSN}/\tau_{vis}$ is the rate of CCSNe. Deriving the value of R_{CCSN} therefore requires the subtraction of SNR that are the result of Type Ia events from the SNR sample. Maoz & Badenes (2010) estimated the fraction, f_{Ia} , of Type Ia SNR in the sample to be between 0.1 and 0.5. To be definitive, we will adopt an average value of $f_{Ia} = 0.30$ in all our calculations.

Determining the dust yield from CCSNe is complicated by the fact that observations taken shortly after the explosion usually sample only the hot dust, and may therefore be missing any cold dust component that may be hidden in optically thick clumps. Detection of dust during the remnant phase is

necessarily limited to young remnants, before their ejecta has mixed with the ISM.

Spitzer and *Herschel* observations of SNRs opened new spectral windows that cover a wide range of dust temperatures and dust emission features, enabling determination of dust composition and heating mechanisms. Surveys of young, unmixed remnants with these satellites revealed $\sim 0.01 - 0.2 M_{\odot}$ of dust in the ejecta of SNRs such as the Crab Nebula, Cas A, G292+1.8, E0102, and G11.2-0.3 (Koo et al. 2007; Rho et al. 2008; Rho et al. 2009; Sandstrom et al. 2009; Barlow et al. 2010; Ghavamian et al. 2012; Gomez et al. 2012; Temim & Dwek 2013; Arendt et al. 2014).

The largest mass of SN condensed dust was found in SN1987A. *Spitzer* and *Herschel* observations revealed $\sim 0.5 - 0.7 M_{\odot}$ of dust (Matsuura et al. 2011), which was subsequently spatially resolved with ALMA and definitively associated with the expanding SN ejecta (Indebetouw et al. 2014; Zanardo et al. 2014). The large mass of dust found in SN1987A suggests that almost all of the refractory elements precipitated out of the gas and formed dust with nearly 100% efficiency.

The yields presented above suggest that only a fraction of the condensable elements in the ejecta of CCSNe form dust. The separate yields of carbon and silicate dust are only known, with great uncertainty, for select remnants. The uncertainty in the dust composition stems from the fact that most of the dust is cold and emits at far-IR wavelengths where there are no distinguishing solid state features. Using all the information above, we adopt a CCSN dust formation efficiency of 20%, and use the theoretically derived elemental yields Woosley & Weaver (1995) to calculate the dust yield in massive stars. These yields are tabulated for 100% condensation efficiencies in Table 2 of Dwek et al. (2007). We average the yields over a mass function of the form $M_*^{-2.35}$, for stars between $8 - 40 M_{\odot}$. The final IMF-averaged dust yields that we calculate for a 100% condensation efficiency for silicate and carbon grains are $0.5 M_{\odot}$ and $0.15 M_{\odot}$, respectively.

With $R_{CCSN} = f_{Ia} N_{SNR} / \tau_{vis}$ and the visibility times listed in Table 4, we get a CCSN rate of $2.6 \times 10^{-3} \text{ yr}^{-1}$ and $7.8 \times 10^{-4} \text{ yr}^{-1}$ for the LMC and SMC, respectively. The resulting dust injection rates are $1.3 \times 10^{-3} M_{\odot}/\text{yr}$ and $3.9 \times 10^{-4} M_{\odot}/\text{yr}$ for silicates and carbon grains in the LMC, and $3.9 \times 10^{-4} M_{\odot}/\text{yr}$ and $1.2 \times 10^{-4} M_{\odot}/\text{yr}$ for silicate and carbon grains in the SMC. The calculated dust injection rates are listed in Table 5.

6.3. AGB Dust Injection Rates

Low mass stars ($M \leq 8 M_{\odot}$) form dust in their winds during the asymptotic giant branch (AGB) phase of their evolution. The dust is injected into the ISM after the stars evolve off the main sequence (MS). The delayed dust injection rate by AGB stars, $[dM_d(t)/dt]_{agb}$ is given by: Dwek (e.g. 1998); Dwek & Cherchneff (e.g. 2011a); Zhukovska et al. (e.g. 2008); Calura et al. (e.g. 2010):

$$\left[\frac{dM_d(t)}{dt} \right]_{agb} = \int_{m_1}^{m_w} Y_{agb}(m) \frac{\psi[t - \tau_{MS}(m)]}{\langle m \rangle} \phi(m) dm \quad (7)$$

where $\tau_{MS}(m)$ is the MS lifetime of a star of mass m , $\langle m \rangle$ is the IMF-averaged stellar mass, m_1 the mass of the lowest mass star that evolved off the MS by time t , $Y_{agb}(m)$ is the total dust yield in AGB stars, and m_w is the upper mass limit of AGB stars, that is, the lower mass limit of stars that become CCSNe.

Figure 8 shows the carbon and silicate dust yields in AGB stars versus stellar mass. Elemental yields were taken from Karakas & Lattanzio (2007), Nanni et al. (2013), and Marigo (private communication), for a metallicity of $Z = 0.008$. Stars

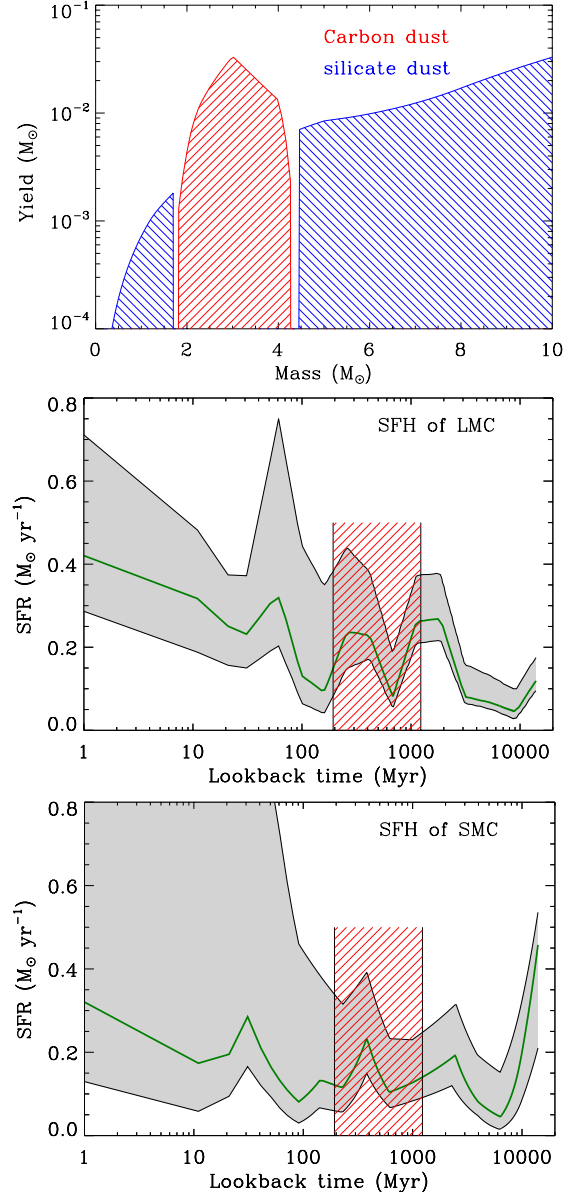


FIG. 8.— **Top:** The dust yield in AGB stars using the Karakas (2010) yields. The yields assume a 100% condensation efficiency in the sources, and that all the carbon (oxygen) is locked up in dust when the C/O ratio is > 1 (< 1). **Middle and bottom:** The star formation histories of the Large and Small Magellanic Clouds after Harris & Zaritsky (2009). The shaded area depicts the birth time of carbon-rich AGB stars that are forming carbon dust at the present epoch.

with C/O ratios > 1 were assumed to produce only carbon dust, and stars with C/O ratios < 1 were assumed to produce only silicate dust. The yields presented in the figure also assume a 100% efficiency in the condensation process. The prescription for calculating the dust yields were presented in Dwek (1998). More realistic models, and a comprehensive comparison of the different AGB yields are presented in Schneider et al. (2014). All models agree that at the LMC metallicity, carbon dust is produced by stars in the $\sim 1.5 - 3.5 M_{\odot}$ mass range, with an average yield of $\sim (1 - 10) \times 10^{-3} M_{\odot}$.

Because of the delay time between the stellar birth and the epoch of dust injection, the dust production rate by AGB stars requires knowledge of the star formation history of the MCs. For sake of consistency with the calculated dust pro-

duction rate by CCSNe, we will first calculate the current SFR in the MCs from the CCSN rate. The relation between the two is given by:

$$\psi = m_* R_{CCSN} \quad (8)$$

Assuming that all stars with masses above $8 M_\odot$ end up as CCSNe (e.g. Heger et al. 2003), the value of m_* depends on the stellar IMF, and is equal to $135 M_\odot$ for a Salpeter, and $90 M_\odot$ for a Kroupa IMF (Dwek & Cherchneff 2011a). For a Salpeter IMF we get that the SFR is $0.35 M_\odot \text{ yr}^{-1}$ and $0.1 M_\odot \text{ yr}^{-1}$ for the LMC and SMC respectively, which is consistent with the values derived by Harris & Zaritsky (2009).

We will therefore adopt their nominal SFH for calculating dust injection rate by AGB stars in the MCs. The middle and bottom panels of Figure 8 show the star formation rate of the LMC and SMC versus lookback time (Harris & Zaritsky 2009). The shaded area depicts the epoch during which carbon stars in the $1.5\text{--}3.5 M_\odot$ mass range contributed to the currently observed injection rate of carbon dust.

Table 5 compares our calculated injection rates of carbon and silicate dust in the LMC and SMC to observations. Not surprisingly, the calculated rates for the LMC are higher by a factor of ~ 5 from the observed range of values, since we adopted a condensation efficiency of 100%. The observations therefore suggest that only $\sim 20\%$ of the refractory elements condense in the ejecta. The discrepancy for the SMC is much higher, suggesting an unusually low condensation efficiency.

7. ASTROPHYSICAL IMPLICATIONS

Table 5 compares the carbon and silicate dust production and destruction rates derived in this paper. The results show that in both the LMC and SMC, the rate of grain destruction by SNRs greatly exceeds the rate of dust injection by AGB stars and CCSNe. This imbalance stems fundamentally from the fact that CCSNe destroy more dust during the remnant phase of their evolution than they produce in their ejecta shortly after core collapse. Only in the very early universe ($z \gtrsim 9$), when the ambient dust-to-gas mass ratio was very low, are SN net producers of interstellar dust (Dwek et al. 2014). This imbalance between the formation and production rates of dust is not limited to the MCs (see also Zhukovska & Henning 2013; Schneider et al. 2014). It also exists in the local solar neighborhood, in galaxies in the local universe (Dwek 1998; Zhukovska et al. 2008; Calura et al. 2010; Galiano et al. 2008), and in the high-redshift universe (Dwek et al. 2007; Valiante et al. 2011; Dwek et al. 2007; Dwek & Cherchneff 2011a; Dwek et al. 2011; Gall et al. 2011a,b; Michalowski et al. 2011).

One possibility for the discrepancy may be due to a significant overestimate of the grain destruction efficiency in the ISM. For example, Jones et al. (1996) find that increasing the density n_0 from 0.25 cm^{-3} to 25 cm^{-3} increases the dust destruction efficiency by up to a factor of two for a shock velocity of 100 km s^{-1} . However, integration over all shock velocities leads to a net increase in the dust destruction rate of only a few percent (Slavin, private communication, in preparation). A larger uncertainty is likely caused by the assumed initial grain size distribution, since any weighting towards the smaller grains would lead to a higher dust destruction efficiency. Another reason for an overestimate of the dust lifetime may be due to our assumption that the SNRs expand into a homogeneous ISM. SNR expanding in a three-phase ISM, dominated by a low-density hot gas will leave most of the dust residing in the dense phase of the ISM intact (Dwek & Scalo 1979; Dwek et al. 2007), but since molecular gas

constitutes only 10% of the gas mass in the MCs, this effect should not significantly increase the dust lifetime. More detailed models following the destruction of dust in a clumpy medium are currently being performed by Slavin (2014).

Alternatively, most dust giving rise to the observed IR emission in these galaxies might have grown by accretion onto surviving thermally-condensed cores in the dense ISM. This possibility is supported by the positive correlation between an element's condensation temperature and interstellar depletion (Field 1974), that may also be interpreted as a trend reflecting the accretion efficiency in molecular clouds (Snow 1975). The composition of interstellar dust must therefore reflect that of composite interstellar grains, composed of refractory silicate or carbon cores and accreted refractory organic material (Greenberg et al. 1995; Li & Greenberg 1997; Zubko et al. 2004; Jones et al. 2013). Models consisting of composite dust have been successful in reproducing the observed interstellar extinction, diffuse IR emission, and interstellar abundance constraints in the local solar neighborhood (Zubko et al. 2004). Such dust model will require the reevaluation of dust destruction rates and lifetimes, and the inclusion of accretion as an additional source of dust.

8. SUMMARY

We calculated the rate of grain destruction by SNRs in the LMC and SMC by modeling the evolution for a nearly complete sample of SNRs, using observationally determined values for the gas density and dust content around each SNR. We find that the average dust mass destroyed by an SNR is $6.1 \pm 2.6 M_\odot$ (1.6 ± 0.7) of silicate (carbon) dust in the LMC, and $2.7 \pm 1.5 M_\odot$ ($0.6 \pm 0.3 M_\odot$) of silicate (carbon) dust in the SMC. The quoted values assume a disk thickness of 0.4 kpc for the LMC, and 2.0 kpc for the SMC, and an average metallicity factor for the MCs of $\zeta_m = 0.3$. The derived dust lifetimes are $22 \pm 13 \text{ Myr}$ ($30 \pm 17 \text{ Myr}$) for silicate (carbon) grains in the LMC, and $54 \pm 32 \text{ Myr}$ ($72 \pm 43 \text{ Myr}$) for silicate (carbon) grains in the SMC. These values correspond to dust destruction rates of $(2.3 \pm 1.3) \times 10^{-2} M_\odot \text{ yr}^{-1}$ ($(5.9 \pm 3.4) \times 10^{-3} M_\odot \text{ yr}^{-1}$) for silicate (carbon) grains in the LMC, and $(3.0 \pm 1.8) \times 10^{-3} M_\odot \text{ yr}^{-1}$ ($(5.6 \pm 3.3) \times 10^{-4} M_\odot \text{ yr}^{-1}$) for silicate (carbon) grains in the SMC. The dust lifetimes and dust destruction rates in the MCs have a $n_0^{-0.464} \zeta_m^{-0.207}$ and $n_0^{0.464} \zeta_m^{0.207}$ dependence on the gas density and metallicity of the ISM into which the SNRs expand, respectively.

We also show that in general, the effective swept-up gas mass \bar{m}_g has a $n_0^{-0.107} \zeta_m^{-0.15}$ dependence on gas density and metallicity. The dependence of the dust lifetime and destruction rate on \bar{m}_g and these parameters should be taken into account in any future dust evolution models.

The dust lifetimes for the MCs are several times lower than those for the Milky Way, which can be explained by the combined effect of the lower total dust mass in the MCs, but also the fact that the isolated SNRs that have the most impact on dust destruction occur in regions with higher than average D2G mass ratios. We find that the derived dust destruction rates are an order of magnitude larger than our estimates of the maximum dust injection rates from AGB stars and core-collapse SNe, implying that dust growth by accretion in the ISM may be important in explaining the current IR emission in the MCs and other galaxies.

We thank Rick Arendt, Jon Slavin, Xander Tielens, Eric Pellegrini, and the participants of the MEGASage 7 collaboration meeting for the useful discussions that helped improve the paper. This work was supported by the NASA ADAP program NNN12ZDA001N-ADAP (proposal ID: 12-ADAP12-0145).

REFERENCES

- Arendt, R. G., Dwek, E., Kober, G., Rho, J., & Hwang, U. 2014, *ApJ*, 786, 55
- Arendt, R. G., Dwek, E., Blair, W. P., et al. 2010, *ApJ*, 725, 585
- Badenes, C., Maoz, D., & Draine, B. T. 2010, *MNRAS*, 407, 1301
- Barlow, M. J., Krause, O., Swinyard, B. M., et al. 2010, *A&A*, 518, L138+
- Bernard, J.-P., Reach, W. T., Paradis, D., et al. 2008, *AJ*, 136, 919
- Blair, W. P., Ghavamian, P., Long, K. S., et al. 2007, *ApJ*, 662, 998
- Blair, W. P., Ghavamian, P., Sankrit, R., & Danforth, C. W. 2006, *ApJS*, 165, 480
- Borkowski, K. J., Williams, B. J., Reynolds, S. P., et al. 2006, *ApJ*, 642, L141
- Bot, C., Ysard, N., Paradis, D., et al. 2010, *A&A*, 523, A20
- Boyer, M. L., Sargent, B., van Loon, J. T., et al. 2010, *A&A*, 518, L142
- Boyer, M. L., Srinivasan, S., Riebel, D., et al. 2012, *ApJ*, 748, 40
- Calura, F., Recchi, S., Matteucci, F., & Kroupa, P. 2010, *MNRAS*, 406, 1985
- Cappellaro, E. 1996, in *IAU Symposium*, Vol. 171, *New Light on Galaxy Evolution*, ed. R. Bender & R. L. Davies, 81
- Chu, Y.-H., & Kennicutt, Jr., R. C. 1988, *AJ*, 95, 1111
- Cioffi, D. F., McKee, C. F., & Bertschinger, E. 1988, *ApJ*, 334, 252
- Dickey, J., Marx, M., & Mebold, U. 1993, in *Astronomische Gesellschaft Abstract Series*, Vol. 9, *Astronomische Gesellschaft Abstract Series*, ed. G. Klare, 25
- Dwek, E. 1998, *ApJ*, 501, 643
- Dwek, E., & Cherchneff, I. 2011a, *ApJ*, 727, 63
- . 2011b, *ApJ*, 727, 63
- Dwek, E., Galliano, F., & Jones, A. P. 2007, *ApJ*, 662, 927
- Dwek, E., & Scalo, J. M. 1979, *ApJ*, 233, L81
- . 1980, *ApJ*, 239, 193
- Dwek, E., Staguhn, J., Arendt, R. G., et al. 2014, *ApJ*, 788, L30
- Dwek, E., Staguhn, J. G., Arendt, R. G., et al. 2011, *ApJ*, 738, 36
- Field, G. B. 1974, *ApJ*, 187, 453
- Filipović, M. D., Payne, J. L., Reid, W., et al. 2005, *MNRAS*, 364, 217
- Gall, C., Andersen, A. C., & Hjorth, J. 2011a, *A&A*, 528, A13+
- . 2011b, *A&A*, 528, A14+
- Galliano, F., Dwek, E., & Chianal, P. 2008, *ApJ*, 672, 214
- Ghavamian, P., Long, K. S., Blair, W. P., et al. 2012, *ApJ*, 750, 39
- Gomez, H. L., Krause, O., Barlow, M. J., et al. 2012, *ApJ*, 760, 96
- Gomez, H. L., Clark, C. J. R., Nozawa, T., et al. 2012, *Monthly Notices of the Royal Astronomical Society*, 420, 3557
- Gordon, K. D., Roman-Duval, J., Bot, C., et al. 2014, *arXiv:1406.6066*
- Greenberg, J. M., Li, A., Mendoza-Gomez, C. X., et al. 1995, *ApJ*, 455, L177+
- Harris, J., & Zaritsky, D. 2004, *AJ*, 127, 1531
- . 2009, *AJ*, 138, 1243
- Haschke, R., Grebel, E. K., & Duffau, S. 2012a, *AJ*, 144, 106
- . 2012b, *AJ*, 144, 107
- Indebetouw, R., Matsuura, M., Dwek, E., et al. 2014, *ApJ*, 782, L2
- Jones, A. P., Fanciullo, L., Köhler, M., et al. 2013, *A&A*, 558, A62
- Jones, A. P., & Nuth, J. A. 2011, *A&A*, 530, A44+
- Jones, A. P., Tielens, A. G. G. M., & Hollenbach, D. J. 1996, *ApJ*, 469, 740
- Jones, A. P., Tielens, A. G. G. M., Hollenbach, D. J., & McKee, C. F. 1994, *ApJ*, 433, 797
- Karakas, A., & Lattanzio, J. C. 2007, *Publications of the Astronomical Society of Australia*, 24, 103
- Karakas, A. I. 2010, *MNRAS*, 403, 1413
- Kim, S., Dopita, M. A., Staveley-Smith, L., & Bessell, M. S. 1999, *AJ*, 118, 2797
- Koo, B.-C., Moon, D.-S., Lee, H.-G., Lee, J.-J., & Matthews, K. 2007, *ApJ*, 657, 308
- Lakićević, M., van Loon, J. T., Meixner, M., et al. 2014, *arXiv:1410.5709*
- Leroy, A., Bolatto, A., Stanimirovic, S., et al. 2007, *ApJ*, 658, 1027
- Li, A., & Draine, B. T. 2002, *ApJ*, 576, 762
- Li, A., & Greenberg, J. M. 1997, *A&A*, 323, 566
- Maggi, P., Haberl, F., Kavanagh, P. J., et al. 2014, *A&A*, 561, A76
- Maoz, D., & Badenes, C. 2010, *MNRAS*, 407, 1314
- Matsuura, M., Woods, P. M., & Owen, P. J. 2013, *MNRAS*, 429, 2527
- Matsuura, M., Barlow, M. J., Zijlstra, A. A., et al. 2009, *MNRAS*, 396, 918
- Matsuura, M., Dwek, E., Meixner, M., et al. 2011, *Science*, 333, 1258
- Meixner, M., Panuzzo, P., Roman-Duval, J., et al. 2013, *AJ*, 146, 62
- Michalowski, M. J., Murphy, E. J., Hjorth, J., et al. 2011, in *Astronomical Society of the Pacific Conference Series*, Vol. 446, *Galaxy Evolution: Infrared to Millimeter Wavelength Perspective*, ed. W. Wang, J. Lu, Z. Luo, Z. Yang, H. Hua, & Z. Chen, 387
- Nanni, A., Bressan, A., Marigo, P., & Girardi, L. 2013, *MNRAS*, 434, 2390
- Nozawa, T., Maeda, K., Kozasa, T., et al. 2011, *ApJ*, 736, 45
- Rana, N. C. 1991, *ARA&A*, 29, 129
- Raymond, J. C., Ghavamian, P., Williams, B. J., et al. 2013, *ApJ*, 778, 161
- Rho, J., Kozasa, T., Reach, W. T., et al. 2008, *ApJ*, 673, 271
- Rho, J., Reach, W. T., Tappe, A., et al. 2009, *Cosmic Dust - Near and Far ASP Conference Series*, 414, 22
- Riebel, D., Srinivasan, S., Sargent, B., & Meixner, M. 2012, *ApJ*, 753, 71
- Roman-Duval, J. et al. *ApJ*, in press
- Sandstrom, K. M., Bolatto, A. D., Stanimirović, S., Loon, J. T. V., & Smith, J. D. T. 2009, *ApJ*, 696, 2138
- Sankrit, R., Williams, B. J., Borkowski, K. J., et al. 2010, *ApJ*, 712, 1092
- Schaefer, B. E. 2008, *AJ*, 135, 112
- Schneider, R., Valiante, R., Ventura, P., et al. 2014, *MNRAS*, 442, 1440
- Seab, C. G., & Shull, J. M. 1983, *ApJ*, 275, 652
- Seok, J. Y., Koo, B.-C., & Onaka, T. 2013, *ApJ*, 779, 134
- Slavin, J. D. 2014, in *American Astronomical Society Meeting Abstracts*, Vol. 224, *American Astronomical Society Meeting Abstracts #224, #220.16*
- Snow, Jr., T. P. 1975, *ApJ*, 202, L87
- Srinivasan, S., Meixner, M., Leitherer, C., et al. 2009, *AJ*, 137, 4810
- Stanimirovic, S., Staveley-Smith, L., Dickey, J. M., Sault, R. J., & Snowden, S. L. 1999, *MNRAS*, 302, 417
- Stanimirović, S., Staveley-Smith, L., & Jones, P. A. 2004, *ApJ*, 604, 176
- Staveley-Smith, L., Sault, R. J., Hatzidimitriou, D., Kesteven, M. J., & McConnell, D. 1997, *MNRAS*, 289, 225
- Szewczyk, O., Pietrzyński, G., Gieren, W., et al. 2009, *AJ*, 138, 1661
- Tammann, G. A., Loeffler, W., & Schroeder, A. 1994, *ApJS*, 92, 487
- Tchernyshyov, K. et al. *ApJ*, submitted
- Temim, T., & Dwek, E. 2013, *ApJ*, 774, 8
- Tielens, A. G. G. M. 1998, *ApJ*, 499, 267
- Valiante, R., Schneider, R., Bianchi, S., & Andersen, A. C. 2009, *MNRAS*, 397, 1661
- Valiante, R., Schneider, R., Salvadori, S., & Bianchi, S. 2011, *MNRAS*, 416, 1916
- Vancura, O., Raymond, J. C., Dwek, E., et al. 1994, *ApJ*, 431, 188
- Williams, B. J., Borkowski, K. J., Ghavamian, P., et al. 2013, *ApJ*, 770, 129
- Williams, B. J., Borkowski, K. J., Reynolds, S. P., et al. 2012, *ApJ*, 755, 3
- Williams, B. J., Borkowski, K. J., Reynolds, S. P., et al. 2006, *ApJ*, 652, L33
- . 2011, *ApJ*, 729, 65
- Williams, R. M., Chu, Y.-H., Dickel, J. R., et al. 1999, *ApJS*, 123, 467
- Winkler, P. F., Williams, B. J., Blair, W. P., et al. 2013, *ApJ*, 764, 156
- Woosley, S. E., & Weaver, T. A. 1995, *ApJS*, 101, 181

- Zanardo, G., Staveley-Smith, L., Ng, C.-Y., et al. 2014, in IAU Symposium, Vol. 296, IAU Symposium, ed. A. Ray & R. A. McCray, 23–26
- Zhukovska, S., Gail, H., & Tieloff, M. 2008, A&A, 479, 453
- Zhukovska, S., & Henning, T. 2013, A&A, 555, A99
- Zubko, V., Dwek, E., & Arendt, R. G. 2004, ApJS, 152, 211
- Zubko, V. G., Mennella, V., Colangeli, L., & Bussoletti, E. 1996, MNRAS, 282, 1321

TABLE 1
PARAMETERS FOR THE LMC SNRS

SNR	Name	Position		D (")	N_H (10^{21}cm^{-2})	D2G (10^{-3})	n_0 (cm^{-3})	$m_g(M_\odot)$		$m_d(M_\odot)$	
		RA	Dec.					Si	C	Si	C
J0448.4-6660	...	04h 48m 22s	-66d 59m 52s	220	1.59	2.07	1.28	1889	1411	2.9	0.7
J0449.3-6920	...	04h 49m 20s	-69d 20m 20s	133	2.98	5.85	2.41	1764	1316	7.7	2.0
J0449.7-6922	B0449-693	04h 49m 40s	-69d 21m 49s	120	3.30	5.92	2.67	1744	1301	7.7	2.0
J0450.2-6922	B0450-6927	04h 50m 15s	-69d 22m 12s	210	2.77	5.78	2.24	1778	1326	7.6	2.0
J0450.4-7050	B0450-709	04h 50m 27s	-70d 50m 15s	357	1.33	2.87	1.08	1925	1439	4.1	1.1
J0453.2-6655	N4	04h 53m 14s	-66d 55m 13s	252	2.07	5.03	1.68	1835	1370	6.9	1.8
J0453.6-6829	B0453-685	04h 53m 38s	-68d 29m 27s	120	1.72	2.87	1.39	1873	1399	4.0	1.0
J0453.9-7000	B0454-7005	04h 53m 52s	-70d 00m 13s	420	0.75	3.03	0.60	2047	1531	4.6	1.2
J0454.6-6713	N9	04h 54m 33s	-67d 13m 13s	177	1.44	4.03	1.17	1909	1426	5.7	1.5
J0454.8-6626	N11L	04h 54m 49s	-66d 25m 32s	87	3.24	4.17	2.63	1748	1303	5.4	1.4
J0455.6-6839	N86	04h 55m 37s	-68d 38m 47s	348	1.73	3.82	1.40	1872	1398	5.3	1.4
J0459.9-7008	N186D	04h 59m 55s	-70d 07m 52s	150	0.99	4.98	0.80	1987	1486	7.3	1.9
J0505.7-6753	DEM L71	05h 05m 42s	-67d 52m 39s	72	1.27	2.75	1.03	1934	1445	4.0	1.0
J0505.9-6802	N23	05h 05m 55s	-68d 01m 47s	111	1.86	4.44	1.51	1857	1387	6.1	1.6
J0506.1-6541	...	05h 06m 05s	-65d 41m 08s	408	1.49	2.48	1.21	1902	1421	3.5	0.9
J0506.8-7026	B0507-7029	05h 06m 50s	-70d 25m 53s	330	0.75	3.76	0.61	2046	1530	5.7	1.5
J0508.8-6831	...	05h 08m 49s	-68d 30m 41s	108	2.55	5.00	2.06	1795	1339	6.7	1.7
J0509.0-6844	N103Bk	05h 08m 59s	-68d 43m 35s	28	3.17	7.81	2.57	1752	1307	10.2	2.6
J0509.5-6731	B0509-67.5	05h 09m 31s	-67d 31m 17s	29	1.11	1.56	0.90	1963	1467	2.3	0.6
J0511.2-6759	...	05h 11m 11s	-67d 59m 07s	108	1.94	2.32	1.57	1849	1381	3.2	0.8
J0513.2-6912	DEM L109	05h 13m 14s	-69d 12m 20s	215	2.23	4.61	1.81	1821	1359	6.2	1.6
J0514.3-6840	...	05h 14m 15s	-68d 40m 14s	218	2.04	2.32	1.65	1838	1372	3.2	0.8
J0517.2-6759	...	05h 17m 10s	-67d 59m 03s	270	2.09	3.91	1.69	1834	1369	5.3	1.4
J0518.7-6939	N120	05h 18m 41s	-69d 39m 12s	134	2.08	6.41	1.68	1834	1370	8.7	2.3
J0519.6-6902	B0519-690	05h 19m 35s	-69d 02m 09s	31	1.20	2.62	0.97	1946	1454	3.8	1.0
J0519.7-6926	B0520-694	05h 19m 44s	-69d 26m 08s	174	1.84	3.11	1.49	1858	1388	4.3	1.1
J0521.6-6543	...	05h 21m 39s	-65d 43m 07s	90	0.66	7.09	0.53	2075	1552	10.9	2.8
J0523.1-6753	N44	05h 23m 07s	-67d 53m 12s	228	3.20	6.21	2.60	1750	1305	8.1	2.1
J0524.3-6624	DEM L175a	05h 24m 20s	-66d 24m 23s	234	3.05	4.24	2.47	1760	1313	5.5	1.4
J0525.1-6938	N132D	05h 25m 04s	-69d 38m 24s	114	1.74	8.26	1.41	1870	1397	11.5	3.0
J0525.4-6559	N49B	05h 25m 25s	-65d 59m 19s	168	2.50	4.20	2.02	1798	1342	5.6	1.4
J0526.0-6605	N49	05h 26m 00s	-66d 04m 57s	84	4.10	6.25	3.32	1703	1269	7.9	2.0
J0527.6-6912	B0528-692	05h 27m 39s	-69d 12m 04s	147	0.83	3.57	0.67	2024	1514	5.4	1.4
J0527.9-6550	DEM L204	05h 27m 54s	-65d 49m 38s	303	1.42	3.08	1.15	1911	1428	4.4	1.1
J0527.9-6714	B0528-6716	05h 27m 56s	-67d 13m 40s	196	0.98	3.40	0.80	1988	1486	5.0	1.3
J0528.1-7038	B0528-7038	05h 28m 03s	-70d 37m 40s	60	0.77	3.85	0.62	2041	1527	5.8	1.5
J0528.3-6714	HP99498	05h 28m 20s	-67d 13m 40s	97	0.92	3.11	0.74	2002	1497	4.6	1.2
J0529.1-6833	DEM L203	05h 29m 05s	-68d 32m 30s	667	1.90	5.71	1.54	1852	1383	7.9	2.0
J0529.9-6701	DEM L214	05h 29m 51s	-67d 01m 05s	100	0.69	2.85	0.56	2064	1544	4.4	1.1
J0530.7-7008	DEM L218	05h 30m 40s	-70d 07m 30s	213	1.23	1.85	1.00	1940	1450	2.7	0.7
J0531.9-7100	N206	05h 31m 56s	-71d 00m 19s	192	1.94	4.95	1.57	1848	1380	6.8	1.8
J0532.5-6732	B0532-675	05h 32m 30s	-67d 31m 33s	252	1.61	5.52	1.30	1886	1409	7.7	2.0
J0534.0-6955	B0534-699	05h 34m 02s	-69d 55m 03s	114	2.30	2.69	1.86	1815	1355	3.6	0.9
J0534.3-7033	DEM L238	05h 34m 18s	-70d 33m 26s	180	1.57	1.31	1.27	1891	1413	1.8	0.5
J0535.5-6916	SNR1987A	05h 35m 28s	-69d 16m 11s	2	1.86	4.15	1.51	1856	1386	5.7	1.5
J0535.7-6602	N63A	05h 35m 44s	-66d 02m 14s	66	1.24	9.62	1.00	1939	1449	13.9	3.6
J0535.8-6918	Honeycomb	05h 35m 46s	-69d 18m 02s	102	2.28	5.03	1.84	1817	1356	6.8	1.8
J0536.1-6735	DEM L241	05h 36m 03s	-67d 34m 36s	135	3.21	6.62	2.60	1750	1305	8.6	2.2
J0536.1-7039	DEM L249	05h 36m 07s	-70d 38m 37s	180	2.54	2.29	2.06	1795	1340	3.1	0.8
J0536.2-6912	B0536-6914	05h 36m 09s	-69d 11m 53s	480	3.28	5.68	2.66	1745	1301	7.4	1.9
J0537.4-6628	DEM L256	05h 37m 27s	-66d 27m 50s	204	1.92	6.94	1.55	1850	1382	9.5	2.5
J0537.6-6920	B0538-6922	05h 37m 37s	-69d 20m 23s	169	3.43	4.69	2.78	1737	1295	6.1	1.6
J0537.8-6910	N157B	05h 37m 46s	-69d 10m 28s	102	5.35	9.17	4.33	1654	1232	11.3	2.9
J0538.2-6922	0538-693	05h 38m 14s	-69d 21m 36s	169	3.67	5.00	2.97	1724	1285	6.4	1.7
J0540.0-6944	N159	05h 39m 59s	-69d 44m 02s	78	6.33	10.4	5.12	1622	1207	12.5	3.2
J0540.2-6920	B0540-693	05h 40m 11s	-69d 19m 55s	60	4.72	4.78	3.82	1676	1249	6.0	1.5
J0543.1-6858	DEM L299	05h 43m 08s	-68d 58m 18s	318	4.73	3.39	3.83	1676	1249	4.2	1.1
J0547.0-6943	DEM L316B	05h 46m 59s	-69d 42m 50s	84	5.88	4.85	4.76	1635	1217	5.9	1.5
J0547.4-6941	DEM L316A	05h 47m 22s	-69d 41m 26s	56	6.20	4.44	5.02	1626	1210	5.4	1.4
J0547.8-7025	B0548-704	05h 47m 49s	-70d 24m 54s	102	3.45	2.54	2.80	1735	1294	3.3	0.8
J0550.5-6823	...	05h 50m 30s	-68d 22m 40s	312	2.62	3.10	2.12	1789	1335	4.1	1.1

NOTE. — Listed values for the density (n_0), effective swept-up gas mass (m_g), and destroyed dust mass (m_d) assume a gas disk thickness of 0.4 kpc. Of the total D2G mass ratio, 74% is attributed to silicates, and 26% to carbon dust.

TABLE 2
PARAMETERS FOR THE SMC SNRS

SNR	Name	Position		D (")	N_H (10^{21}cm^{-2})	D2G (10^{-3})	n_0 (cm^{-3})	$m_g(M_\odot)$		$m_d(M_\odot)$	
		RA	Dec.					Si	C	Si	C
J0040.9-7337	DEM S5	00h 40m 55s	-73d 36m 55s	121	3.17	0.50	0.51	2082	1558	0.8	0.2
J0046.6-7309	DEM S32	00h 46m 39s	-73d 08m 39s	136	10.30	1.61	1.67	1836	1371	2.4	0.4
J0047.2-7308	IKT2	00h 47m 12s	-73d 08m 26s	66	10.89	1.76	1.76	1825	1363	2.6	0.5
J0047.5-7306	B0045-733	00h 47m 29s	-73d 06m 01s	180	10.58	1.80	1.71	1831	1367	2.7	0.5
J0047.7-7310	HFPK419	00h 47m 41s	-73d 09m 30s	90	10.66	1.96	1.73	1829	1366	2.9	0.5
J0047.8-7317	NS21	00h 47m 48s	-73d 17m 27s	76	9.66	2.42	1.56	1849	1381	3.6	0.7
J0048.1-7309	NS19	00h 48m 06s	-73d 08m 43s	79	11.65	2.25	1.89	1812	1352	3.3	0.6
J0048.4-7319	IKT4	00h 48m 25s	-73d 19m 24s	84	8.98	1.87	1.46	1864	1392	2.8	0.5
J0049.1-7314	IKT5	00h 49m 07s	-73d 14m 05s	116	9.11	1.64	1.48	1861	1390	2.5	0.5
J0051.1-7321	IKT6	00h 51m 07s	-73d 21m 26s	144	6.98	1.29	1.13	1915	1431	2.0	0.4
J0051.9-7310	IKT7	00h 51m 54s	-73d 10m 24s	97	7.23	1.43	1.17	1908	1425	2.2	0.4
J0052.6-7238	B0050-728	00h 52m 33s	-72d 37m 35s	323	4.89	0.96	0.79	1989	1487	1.5	0.3
J0058.3-7218	IKT16	00h 58m 16s	-72d 18m 05s	200	5.69	1.41	0.92	1957	1463	2.2	0.4
J0059.4-7210	IKT18	00h 59m 25s	-72d 10m 10s	158	3.92	2.26	0.64	2036	1523	3.7	0.7
J0100.3-7134	DEM S108	01h 00m 21s	-71h 33m 40s	149	3.06	1.55	0.50	2090	1563	2.6	0.5
J0103.2-7209	IKT21	01h 03m 13s	-72d 08m 59s	62	5.48	1.48	0.89	1965	1469	2.3	0.4
J0103.5-7247	HFPK334	01h 03m 30s	-72d 47m 20s	86	4.35	0.74	0.70	2014	1506	1.2	0.2
J0104.0-7202	B0102-7219	01h 04m 02s	-72d 01m 48s	44	5.24	2.11	0.85	1975	1476	3.3	0.6
J0105.1-7223	IKT23	01h 05m 04s	-72d 22m 56s	170	4.13	0.91	0.67	2025	1515	1.5	0.3
J0105.4-7209d	DEM S128	01h 05m 23s	-72d 09m 26s	124	4.66	1.35	0.75	1999	1495	2.2	0.4
J0105.6-7204	DEM S130	01h 05m 39s	-72d 03m 41s	79	5.61	1.76	0.91	1960	1465	2.8	0.5
J0106.2-7205	IKT25	01h 06m 14s	-72d 05m 18s	110	5.58	1.43	0.90	1961	1466	2.3	0.4
J0114.0-7317	N83C	01h 14m 00s	-73d 17m 08s	17	5.50	5.41	0.89	1965	1468	8.5	1.6

NOTE. — Listed values for the density (n_0), effective swept-up gas mass (m_g), and destroyed dust mass (m_d) assume a gas disk thickness of 2.0 kpc. Of the total D2G mass ratio, 80% is attributed to silicates, and 20% to carbon dust.

TABLE 3
AVERAGE VALUES VS. DISK THICKNESS

d (kpc)	\bar{n}_0 (cm^{-3})	\bar{R}_{SN} (10^{-3}yr^{-1})	$\bar{m}_g(M_\odot)$		$\bar{m}_d(M_\odot)$		$\tau_d(\text{Myr})$		$dM_d(t)/dt$ ($10^{-3} M_\odot/\text{yr}$)	
			Si	C	Si	C	Si	C	Si	C
LMC										
0.1	7.6 ± 4.4	8.29 ± 3.17	1580 ± 103	1174 ± 80	5.2 ± 2.2	1.3 ± 0.6	12 ± 7	16 ± 9	43.3 ± 25	11.1 ± 6.3
0.2	3.8 ± 2.2	5.58 ± 2.13	1709 ± 108	1273 ± 83	5.7 ± 2.4	1.5 ± 0.6	16 ± 9	22 ± 13	31.5 ± 18	8.1 ± 4.6
0.4	1.9 ± 1.1	3.75 ± 1.44	1843 ± 114	1376 ± 87	6.1 ± 2.6	1.6 ± 0.7	22 ± 13	30 ± 17	22.9 ± 13	5.9 ± 3.4
0.7	1.1 ± 0.6	2.73 ± 1.04	1957 ± 118	1463 ± 90	6.5 ± 2.7	1.7 ± 0.7	29 ± 17	39 ± 22	17.7 ± 10	4.6 ± 2.6
1.6	0.5 ± 0.3	1.70 ± 0.65	2133 ± 123	1594 ± 91	7.1 ± 3.0	1.8 ± 0.8	43 ± 25	57 ± 33	12.0 ± 6.8	3.1 ± 1.8
SMC										
0.7	3.2 ± 1.3	2.03 ± 0.50	1728 ± 79	1289 ± 60	2.4 ± 1.3	0.45 ± 0.24	33 ± 20	44 ± 27	4.9 ± 2.9	0.90 ± 0.54
1.0	2.2 ± 0.9	1.65 ± 0.41	1797 ± 81	1341 ± 62	2.5 ± 1.4	0.46 ± 0.25	39 ± 24	52 ± 32	4.1 ± 2.5	0.77 ± 0.46
2.0	1.1 ± 0.5	1.11 ± 0.27	1937 ± 85	1447 ± 65	2.7 ± 1.5	0.50 ± 0.27	54 ± 32	72 ± 43	3.0 ± 1.8	0.56 ± 0.33
4.0	0.6 ± 0.2	0.75 ± 0.19	2083 ± 89	1558 ± 67	2.9 ± 1.6	0.54 ± 0.29	74 ± 45	99 ± 60	2.2 ± 1.3	0.40 ± 0.24
5.0	0.4 ± 0.2	0.66 ± 0.16	2132 ± 89	1594 ± 67	3.0 ± 1.6	0.55 ± 0.30	82 ± 50	110 ± 67	1.9 ± 1.2	0.36 ± 0.22

NOTE. — The uncertainties in n_0 , \bar{m}_g and \bar{m}_d represent the standard deviation, uncertainty on \bar{R}_{SN} reflects the spread in visibility times τ_v for all SNRs in the sample. The uncertainties were propagated accordingly for the rest of the parameters, based on equations is §2.

TABLE 4
DERIVED PARAMETERS

Parameter	Density Dependence	Metallicity Dependence	LMC		SMC	
			Silicates	Carbon	Silicates	Carbon
\bar{n}_0 around SNRs (cm^{-3})	1.9 ± 1.1		1.1 ± 0.5	
$\overline{D2G}$ around SNRs (10^{-3})	4.5 ± 2.0		1.7 ± 0.9	
$\overline{D2G}$ global (10^{-3})	1.8		0.8	
$\bar{\tau}_{vis}$ (kyr)	$n_0^{-4/7}$	$\zeta_m^{-5/14}$	16.3		20.7	
\bar{R}_{SN} ($10^{-3} M_\odot/\text{yr}$)	$n_0^{4/7}$	$\zeta_m^{5/14}$	3.75 ± 1.44		1.11 ± 0.27	
M_d ($10^5 M_\odot$)	5.2 ± 0.4	1.8 ± 0.1	1.6 ± 0.2	0.40 ± 0.04
T_d (K)	22.4 ± 0.4	26.9 ± 0.5	19.0 ± 0.5	22.8 ± 0.6
$\bar{m}_g (M_\odot)$	$n_0^{-0.107}$	$\zeta_m^{-0.15}$	1840 ± 110	1380 ± 80	1940 ± 90	1450 ± 70
$\bar{m}_d (M_\odot)$	$n_0^{-0.107}$	$\zeta_m^{-0.15}$	6.1 ± 2.6	1.6 ± 0.7	2.7 ± 1.5	0.57 ± 0.27
τ_d (Myr)	$n_0^{-0.464}$	$\zeta_m^{-0.207}$	22 ± 13	30 ± 17	54 ± 32	72 ± 43
$dM_d(t)/dt$ ($10^{-3} M_\odot/\text{yr}$)	$n_0^{0.464}$	$\zeta_m^{0.207}$	23 ± 13	5.9 ± 3.4	3.0 ± 1.8	0.56 ± 0.33

NOTE. — The assumed nominal disk thickness values for the LMC and SMC are 0.4 kpc and 2.0 kpc, respectively, based on estimates of Kim et al. (1999) and Stanimirović et al. (2004). The assumed metallicity factor ζ_m is 0.3. The dependence of the derived parameters on the ambient gas density is indicated in the second column. The disk thickness dependence for each parameter is just the inverse of the density dependence ($n_0 \propto d^{-1}$). We note that density and metallicity dependence for τ_d and $dM_d(t)/dt$ is specific to analyses of galaxies with complete samples of resolved SNRs, since it involves the density and metallicity dependent R_{SN} and τ_{vis} (see Section 5)

TABLE 5
DUST INJECTION AND DESTRUCTION RATES
 $dM_d(t)/dt$ ($10^{-6} M_\odot/\text{yr}$)

Source	LMC		SMC		Reference
	Silicates	Carbon	Silicates	Carbon	
AGB Stars					
	0.95–5.5	9.5–13.6	0.08	0.75	Observed*
	31	108	21	85	This work
Core Collapse SNe					
	1.3×10^3	3.9×10^2	3.9×10^2	1.2×10^2	This work
Destruction by SNe					
	-2.3×10^4	-5.9×10^3	-3.0×10^3	-5.6×10^2	This work

NOTE. — *References for observational measurements of dust injection by AGB stars for the LMC: Srinivasan et al. (2009), Boyer et al. (2012), Riebel et al. (2012), and SMC: Boyer et al. (2012). The dust injection rates from AGB stars and CCSNe estimated in this work assume a 100% grain condensation efficiency, and do not include dust destruction by the SN reverse shock. They therefore represent absolute upper limits on the injected dust mass.